Engineering Geology 157 (2013) 124–132

Contents lists available at SciVerse ScienceDirect

Engineering Geology

journal homepage: www.elsevier.com/locate/enggeo

# The hypermobility of huge landslides and avalanches

Shiva P. Pudasaini [a,b,*], Stephen A. Miller [a]

[a] Department of Geodynamics and Geophysics, Steinmann Institute, University of Bonn, Meckenheimer Allee 176, D-53115, Bonn, Germany
[b] School of Science, Kathmandu University, P. O. Box: 6250, Kathmandu, Nepal

ARTICLE INFO

*Article history:*
Received 13 August 2012
Received in revised form 2 January 2013
Accepted 12 January 2013
Available online 4 February 2013

*Keywords:*
Hypermobility
Huge landslides and avalanches
Terrestrial and extraterrestrial avalanches
Extreme travel distances
Physical modeling and model validation
Fluidization

ABSTRACT

Catastrophic failure of large land masses, which generate landslides, rockfalls and debris avalanches, can have hazardous consequences extending far beyond the source. Observations show that the mobility of such events depends strongly on the volume for volumes larger than $10^6$ m$^3$, with many different processes invoked to explain higher mobilities (hypermobility) for both terrestrial and extraterrestrial events. Although the mobility of large events has been extensively studied, there is no generally accepted mechanism for predicting extreme travel distances because the underlying physical processes are poorly understood. Here we show using physical and rheological arguments that the wide scatter observed for very large mass wasting events in all environments collapses to a single relationship between event volume or inundation area and mobility. Hypermobility is defined to be the reciprocal of the effective friction coefficient $\mu_e$, where the scale-dependent $\mu_e$ is derived analytically as a function of the mechanical, volumetric and topographical parameters of the flow. The dominant term in the coefficient is the degree of fluidization involved in the flow; our results show that fluidization is limited in extraterrestrial events, that significant fluidization occurs in non-volcanic and volcanic events, and fluidization dominates submarine events. This analysis demonstrates that fluidization is associated with long run-out distances, and that the degree of fluidization can be predicted by the volume, and physical and topographic parameters. The methodology is simple, physically-based and validated with datasets of very large terrestrial and extraterrestrial avalanche events. We demonstrate that the effective Coulomb friction rheology and the hypermobility function are applicable to avalanche events of any size, providing an opportunity to simulate past and/or potential huge landslide and debris avalanche events, run-out distances, destructive impact and assessment of risk. The model can be used to estimate the overrun area and volume in terms of known mobility data.

© 2013 Elsevier B.V. All rights reserved.

## 1. Introduction

A major concern in mass flow dynamics is understanding the physical processes operating during large volume landslides, avalanches, debris flows and rock falls with exceptionally long run-out distances (here called hypermobility). The large volume events can generate extremely mobile gravity-driven debris avalanches capable of traveling horizontal runout distances ($L$) as far as 30 times their vertical fall height ($H$) at velocities up to 100 ms$^{-1}$ (Legros, 2002). These events involve up to $10^{12}$ m$^3$ of debris, sometimes traveling hundreds of kilometers over topographic slopes as low as 1° (Shreve, 1966; Howard, 1973; Voight, 1978, 1988; Keefer, 1984; Beget and Kienle, 1992; Siebert, 1992; Dade and Huppert, 1998; Legros, 2002; Sosio et al., 2012). The final debris deposit can be tens to hundreds of meters thick over areas of tens of thousands square kilometers (Howard, 1973; Lucchitta, 1978, 1979; Voight, 1978; Crandell et al., 1984; Keefer, 1984; Francis et al., 1985; Siebert et al., 1987; McEwen, 1989; Beget and Kienle, 1992; Siebert, 1992; Stoopes and Sheridan, 1992; Dade and Huppert, 1998; Legros, 2002; Kelfoun and Druitt, 2005; Davies et al., 2010; Sosio et al., 2011). An extensive list of transport mechanisms has been proposed to explain reduced friction and the hypermobility of large avalanches, including fine powders at the base, interstitial fluids, pore fluid pressure, air pockets, dispersive grain flow, local steam generation, frictionites, lubrication, fluidization, entrainment, oscillation, and dynamic fragmentation (Kent, 1966; Shreve, 1966; Howard, 1973; Hsu, 1975; Lucchitta, 1978, 1979; McSaveney, 1978; Davies, 1982; McEwen, 1989; Iverson, 1997, 2005; Davies and McSaveney, 1999; Legros, 2002; Collins and Melosh, 2003; Campbell, 2006; Mangeney et al., 2007; Pudasaini and Hutter, 2007; Deganutti, 2008; Cagnoli and Quareni, 2009; McSaveney and Davies, 2009; Davies et al., 2010). Although many of these mechanisms are appropriate to some site-specific landslides and debris avalanches, no one dominant mechanism stands out as an explanation for the hypermobility.

Classical mobility approaches (Dade and Huppert, 1998; Calder et al., 1999; Legros, 2002) do not explain the mass-dependence of the

* Corresponding author at: Department of Geodynamics and Geophysics, Steinmann Institute, University of Bonn, Meckenheimer Allee 176, D-53115, Bonn, Germany. Tel.: +49 228 73 24 66.
*E-mail address:* pudasaini@geo.uni-bonn.de (S.P. Pudasaini).

0013-7952/$ – see front matter © 2013 Elsevier B.V. All rights reserved.
http://dx.doi.org/10.1016/j.enggeo.2013.01.012

hypermobility of large avalanche events. Coulomb friction rheology is effective in modeling small volumes (see, e.g., Iverson, 1997; Denlinger and Iverson, 2001; Pitman et al., 2003; Pudasaini and Hutter, 2003; Pudasaini and Kroener, 2008; Pudasaini et al., 2005, 2008; Pudasaini and Domnik, 2009; McDougall and Hungr, 2004; Ancey, 2005; Pitman and Le, 2005; Jop et al., 2006; Mangeney et al., 2007), but modeling large mass flows is inhibited because the appropriate values for the effective friction coefficient and effective stress are unknown and unconstrained (Dade and Huppert, 1998; Legros, 2002; Pudasaini and Hutter, 2007). Furthermore, a realistic rheological model should systematically include the physical, volumetric and topographical effects, and most importantly, determine whether and how the flow rheology depends on the mass. For a moving mass, $H/L$ represents the (scale-free) coefficient of Coulomb sliding friction (Dade and Huppert, 1998; Legros, 2002). The inverse quantity, $L/H$ is the measure of the mobility of the debris avalanches. This mobility is the basic parameter for estimating the areas at risk from debris avalanches, however, field data (see, e.g., Dade and Huppert, 1998; Legros, 2002; Deganutti, 2008; Sosio et al., 2011, 2012) show that simple Coulomb friction fails to predict the large event mobility because the volume of large events must be coupled with the topography of the inundation area and other physical parameters. Since the friction coefficient is substantially reduced during debris avalanches with exceptionally long travel distances, it must explicitly include a length scale, such as volume, inundation area, and topographic constraints. The friction coefficient must also include the intrinsic (true) frictional behavior of the material. In a well-known paper, Dade and Huppert (1998) propose relationships between an assumed uniform triangular inundation area with a constant shear stress ($\tau$) and the loss of potential energy. They estimate a single average value of $\tau$ over datasets of all event types through a regression analysis between energy and area, suggesting a unit value of the geometric parameter $\lambda_{dh}=A/L^2$ (for definition, see Section 2). A drawback in this approach is that estimates of the amount of the work done by the debris during its slide are too high since $\tau$ is applied to the whole overrun area ($A$) and then multiplied by $L$. This leads to much higher values of the effective friction forces than their empirical estimation. Fig. 1 (McDougall and Hungr, 2004) shows that a physically more reasonable approach is to apply $\tau$ only to the (transient) debris covered area $A_t$ (because $\tau$ is zero outside of $A_t$), and then multiplying by the total horizontal travel length $L$. The Dade and Huppert model is restricted to a horizontal triangular (angular) emplacement of the flow as described through the plan-shape geometric parameter $\lambda_{dh}$, and contains $\tau$ (considered a constant) as a fitting parameter that does not necessarily contain a mechanical significance (Dade and Huppert, 1998). Legros (2002) applied the energy equation to this angular geometry and showed that the predicted velocities were substantially higher than observed in real landslides. Additionally, the assumption that $\tau$ is independent of the overburden pressure can be questioned for frictional materials. We mention that, Kelfoun and Druitt (2005) reproduced the Socompa volcanic debris deposit by using a constant basal stress. Recently, Davies et al. (2010) proposed a model for the basal shear stress in terms of the normal stress on the top of the fragmenting layer of the volcanic debris and fragmentation induced dispersive pressure. The model is applied to explain dynamic fragmentation on Socompa volcanic debris avalanche.

In this paper, we construct a model for determining the mean basal shear stress and a mass- or volume-dependent hypermobility and compare the model to available datasets.

## 2. The model

### 2.1. Basal shear stress

We derive the model equations for the mean basal shear stress, effective Coulomb friction coefficient and the hypermobility. We begin

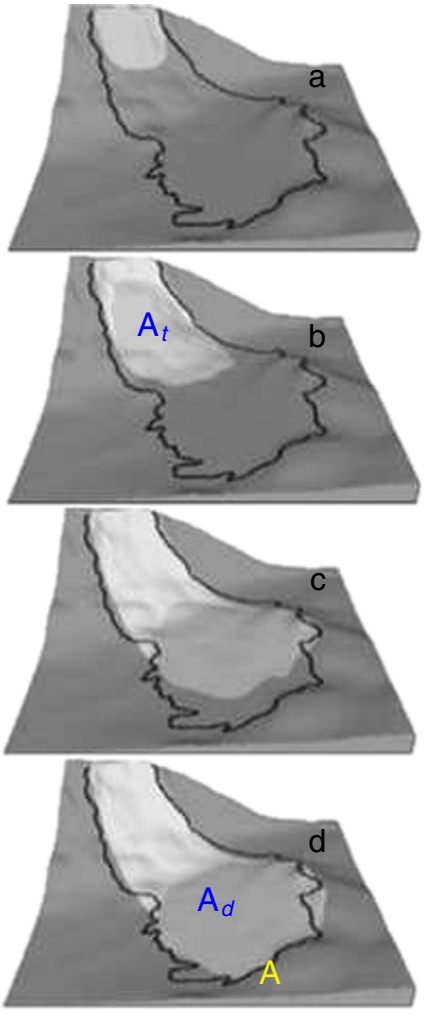


**Fig. 1.** Illustration showing how $A_t \ll A$, using the Frank slide (1903) as an example, where the 30 million $m^3$ slide partially buried the town of Frank, Alberta. The descending mass is in light gray. White area is the passage of the slide. The solid dark line indicates the measured trimline of the inundation area ($A$) of the flow. The simulation time was $t=0$, 20, 40, 60 s, respectively, for panels a, b, c, d (McDougall and Hungr, 2004). Panels a and d show the initial mass and the final deposition. The area beneath the deposited mass is called $A_d$. Panels b and c are the transient sliding mass and the area beneath them is denoted by $A_t$.

with the local dynamical basal shear stress (Iverson, 1997; Iverson and Denlinger, 2001; Pudasaini et al., 2005)

$$\tau_l = \mu_c(1-\Lambda)\ \rho g\ (\cos\zeta + a_c)\ h(t;x,y), \tag{1}$$

where $\mu_c$ is the Coulomb friction coefficient, $\rho$ is the bulk density, $g$ is gravity acceleration, $\zeta$ is the slope angle of the basal surface, $a_c$ accounts for topographically induced centrifugal forces, $h$ is the flow depth in the direction normal to the sliding surface, $t$ is time, and $x$ and $y$ are the downslope and cross-slope coordinates, respectively. $\Lambda$ is associated with the degree of fluidization. That is, $\Lambda$ is the ratio between the pore fluid pressure at the bed and the total normal pressure of the debris mass in the normal direction (Iverson and Denlinger, 2001; Pudasaini et al., 2005). This information can be substantial to (estimate and) predict the hypermobility of large debris avalanches (Berti et al., 1999; Major and Iverson, 1999; Iverson and Vallance, 2001; Berti and Simoni, 2005; McArdell et al., 2007). For more discussion on this, see Section 3. However, $\Lambda$ can be mathematically analogous to the fluid volume fraction (Pudasaini et al., 2005; Pudasaini, 2012), or any other possible mechanism (see, Section 1) that reduces the basal shear resistance such as dynamic fragmentation (McSaveney

and Davies, 2009; Davies et al., 2010). For simplicity, we consider only the basal shear stress and not the complete stress tensor. The total shear force is determined (estimated) by conserving debris mass and integrating Eq. (1) over the inundation area $A$ along the slope,

$$\int_A \tau_l dA = \int_{A_t} \tau_l dA_t \le \mu_c(1-\Lambda)\rho g\left(\cos\zeta_0 + a_{c_0}\right) \int_{A_t} h(t;x,y)dA_t = \mu_c(1-\Lambda)\rho g \mathcal{T}\, V, \tag{2}$$

where $A_t$ is the debris covered area at time $t$, $dA$ is an infinitesimal area in the flow domain $A$ (the entire landslide area), $\zeta_0$ is the minimum of $\zeta$, $a_{c_0}$ is the maximum of $a_c$, $\mathcal{T} = \cos\zeta_0 + a_{c_0}$ is the topographic parameter, and $V$ is the debris volume. Since the debris volume is conserved, $\int_{A_t} h(t;x,y)dA_t = V$. The fact that the debris flow depth $h$, and thus the shear stress $\tau_l$, is zero outside of $A_t$ is utilized to derive Eq. (2). The upper bound of the mean basal shear stress over the typical overrun area $A_t$ is

$$\tau = \frac{1}{A_t}\int_{A_t} \tau_l dA_t \le \mu_c(1-\Lambda)\rho g\mathcal{T}\frac{V}{A_t} \le \mu_c(1-\Lambda)\rho g\mathcal{T}\frac{V}{A_d}, \tag{3}$$

where $A_d$ is the debris coverage area in the deposition (deposition area). The choice of $A_d$ is due to the fact that it is easier to measure than $A_t$. Also note that because of the accumulation of the sliding mass in the deposition area, usually $A_d \le A_t$. If this (upper bound) mean shear stress can describe long run-out avalanches reasonably well, then any other suitable positive value lower than that also qualitatively describes such events. Since the upper bound calculated this way suffices, for simplicity we define ($:=$) the mean basal shear stress as

$$\tau := \mu_c(1-\Lambda)\rho g\mathcal{T}\frac{V}{A_d}. \tag{4}$$

For a mean flow depth $\mathcal{H}$, and assuming a power law proportionality between $V$ and $A$ and a linear relationship between $A$ and $A_d$, we can estimate $\mathcal{H}$ as (see Appendix A for derivation):

$$\mathcal{H} = \gamma_3 A^{n-1}, \tag{5}$$

where $n>1$ is a real number, $\gamma_3 = \gamma_1/\gamma_2 < 1$, $\gamma_1 < \gamma_2 < 1$, and $\gamma_1$, $\gamma_2$ are proportionality constants between $V$ and $A$, and $A$ and $A_d$ with proper dimensions. These assumptions are discussed later and their validity can be evaluated by comparing model predictions with field observation. Eq. (5) means that $\mathcal{H}$ scales with $A^{n-1}$. With Eq. (5) Eq. (4) can now be written as (see Appendix A):

$$\tau = \mu_c(1-\Lambda)\frac{\mathcal{T}}{\gamma_1}\rho g\mathcal{H}\frac{V}{A^n}. \tag{6}$$

Eq. (6) can be used to obtain the non-dimensional friction number $N_f$ (see Appendix B):

$$N_f = \frac{(1-\Lambda)\rho g\mathcal{T}\mathcal{H}}{\tau} = \frac{\gamma_1}{\mu_c}\frac{A^n}{V}. \tag{7}$$

With the definition of the volume-area slope, $S = (N_f\mu_c/\gamma_1)^{1/n}$, a functional relationship between the volume and area can be derived (see Appendix B):

$$A = SV^{1/n}. \tag{8}$$

### 2.2. Effective Coulomb friction coefficient and hypermobility

Balancing between the work ($W = FL$) and the total available energy ($gMH$), we obtain $gMH = FL$, where $M$ is the debris mass and $F$ is the effective friction force (Middleton and Wilcock, 1994; Dade and Huppert, 1998; Pudasaini and Domnik, 2009). The problem remains about how to model $F$. We consider a Coulomb-type friction rheology and apply the shear stress $\tau$, as derived in Eq. (6), to the typical overrun area $A_t$ (or $A_d$), so $F = \tau A_d$. This approach is distinctly different from previous models that argued against Coulomb-type friction (Dade and Huppert, 1998; Calder et al., 1999; Legros, 2002). In their approach, $F = \tau A$, in which $\tau$ is a fit parameter, and $A$ is the projected total inundation area in the horizontal plane, but also restricted to be in the angular sector (see, below). Since $gMH = FL = \tau A_d L$, from Eq. (6), a straightforward calculation yields a relationship between the debris inundation area and the mobility (see Appendix C):

$$\frac{H}{L} \equiv \mu_c(1-\Lambda)\gamma\mathcal{T}\frac{\mathcal{H}}{A^{n-1}} =: \mu_e. \tag{9}$$

We know that $H/L$ is the observed quantity (effective or apparent friction coefficient) that is somehow related to the observed volume ($V_o$) (see, Figure 2). Here, '$o$' stands for observed quantity with discrete distribution. The equivalent expressions (denoted by $\equiv$) in Eq. (9) can be separated as (see Appendix C)

$$\mu_{e_o} := \frac{H}{L}, \tag{10}$$

$$\mu_e = \mu_c(1-\Lambda)\gamma\mathcal{T}\frac{\mathcal{H}}{A^{n-1}}, \tag{11}$$

where $\mu_{e_o}$ is the effective friction coefficient as a function of the observed volume ($V_o$). Combining Eqs. (8) and (9) produces a functional relationship between the debris volume and the theoretical hypermobility (defined as $1/\mu_e$) which can be re-written in terms of $V$ as (see Appendix C):

$$\frac{H}{L} \equiv \frac{\mu_c(1-\Lambda)\gamma\mathcal{T}}{S^{n-1}}\frac{\mathcal{H}}{V^{1-\frac{1}{n}}} = \mu_e. \tag{12}$$

As in Eqs. (10) and (11), equivalent expressions in Eq. (12) can be separated as (see Appendix C)

$$\mu_{e_o} = \frac{H}{L}, \tag{13}$$

$$\mu_e = \frac{\mu_c(1-\Lambda)\gamma\mathcal{T}}{S^{n-1}}\frac{\mathcal{H}}{V^{1-\frac{1}{n}}}. \tag{14}$$

Eq. (14) (similarly, Eq. (11)) represents an explicit and theoretical–empirical functional relation for $\mu_e$ (theoretical effective or apparent friction coefficient) in terms of the (continuous) volume (distribution), $V$. This analytical–empirical model contains several physical and geometrical parameters including, $\mu_c, \Lambda, \gamma, \mathcal{T}, \mathcal{H}, S, n$. The function $\mu_e$ is termed as the theoretical effective Coulomb friction coefficient and its reciprocal, $1/\mu_e$, is called the theoretical hypermobility that describes the long runout of the huge landslides, rock falls, debris flows and avalanches. So, with these notations, $1/\mu_{e_o}$ is the observed hypermobility, whereas $1/\mu_e$ is the theoretical–empirical prediction of the hypermobility. Note that the derived hypermobility expression $1/\mu_e$ is now separated from the field data $\left(1/\mu_{e_o} = L/H\right)$. This is advantageous, because the theoretical hypermobility can now be described independently by the analytical model $\frac{1}{\mu_e} = \frac{S^{n-1}}{\mu_c(1-\Lambda)\gamma\mathcal{T}}\frac{V^{1-\frac{1}{n}}}{\mathcal{H}}$ as a function of the event volume ($V$) and then compared to the field data $\left(1/\mu_{e_o} = L/H\right)$; expressed in terms of the measured volume $V_o$; to test the model.

Since Eqs. (11) and (14) are identical, the flow mobility can be described by either Eq. (11) or by (14). Note that the above equations are valid for any $n>1$. The choice $n = 3/2$ makes $\gamma$ dimensionless (also see, Dade and Huppert, 1998). Such an $n$ value was also observed for long runout rockfalls and debris avalanches (Hungr, 1990; Vallance and Scott, 1997; Dade and Huppert, 1998; Calder et al., 1999; Legros, 2002), but in their approach, $n = 3/2$ resulted from the restricted

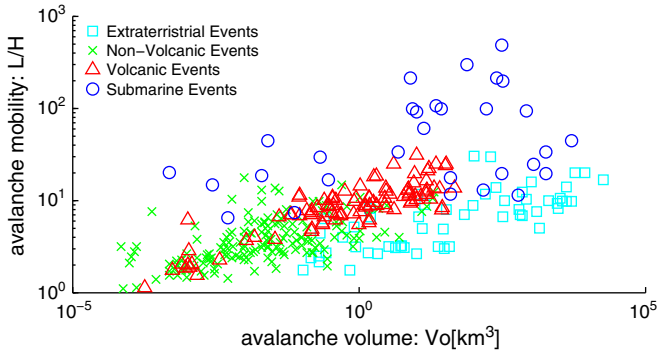


**Fig. 2.** Relationship between the measured avalanche volume ($V_o$) and mobility ($1/\mu_{e_o} = L/H$) for extraterrestrial, non-volcanic, volcanic and submarine events. Data are from (Howard, 1973; Lucchitta, 1978, 1979; Voight, 1978; Crandell et al., 1984; Francis et al., 1985; Siebert et al., 1987; McEwen, 1989; Stoopes and Sheridan, 1992; Dade and Huppert, 1998; Capra et al., 2002; Deganutti, 2008).

form of the overrun area $A = \lambda_{dh} L^2$. To quote Dade and Huppert (1998): "$2\lambda_{dh}$ is the angular extent of the assumed uniform sector through which an avalanche spreads". We do not assume a form of $A$, rather $n = 3/2$ emerges from dimensional analysis. In our approach, since $\tau$ is derived from the physical arguments and is not a fit parameter, our results provide an independent theoretical and physical basis to explain observations.

Eqs. (11) and (14) show that (for $n = 3/2$) the hypermobility ($1/\mu_e$) scales with the square-root of the total overrun area or the cube-root of the debris volume, respectively. For a particular event, $\mathcal{H}$ is usually known or can be estimated from the field observations. However, for a particular event type (e.g., available dataset of all volcanic events; or any other event types) $\mathcal{H}$ is interpolated between the observed minimum and maximum values of $V$ by using an auxiliary thickness distribution function:

$$\mathcal{H} = \mathcal{H}_{min} + (\mathcal{H}_{max} - \mathcal{H}_{min}) \left( \frac{V - V_{min}}{V_{max} - V_{min}} \right)^{\alpha}; \quad V_{min} \le V \le V_{max}, \qquad (15)$$

where $\alpha$ is the shape parameter for the specific event type. Eq. (15) also holds for the inundation area, $A$.

The explicit derivation of $\tau$ from the physical, topographical and the volumetric parameters of the flow event differs from previous models. Previous models do not consider the material friction $\mu_c$, the fluidity parameter $\Lambda$, the topographic parameter $\mathcal{T}$, and volumetric parameter $\gamma$, while previous yield strength estimates (see, e.g., Dade and Huppert, 1998) did not consider Coulomb friction, the mean flow height (Davies et al. (2010) partially include the flow height and friction), and the slope and curvature-induced centrifugal forces that influence the runout. These processes, fundamental to landslide velocity, may be controlled by topographic slope and flow thickness (Legros, 2002; Pudasaini et al., 2005). Estimating the friction number involves the flow depth $\mathcal{H}$ rather than the vertical height drop of the avalanche $H$, and therefore is physically meaningful. That is, for frictional geo-materials the shear stress $\tau$ should be related to $\mathcal{H}$ rather than $H$. Importantly, Eq. (11) or (14) includes the area affected by the flow or the volume and the topographical constraints to explain the hypermobility. The presence of $\mathcal{T}$ in Eq. (11) or (14) implies a positive correlation between the slope (curvature) and the effective friction coefficient as observed in the field and laboratory (Okura et al., 2003; Strom, 2006; Pudasaini and Hutter, 2007; Fischer et al., 2012; Sosio et al., 2012). Lucas and Mangeney (2007) proposed a model in which the intrinsic mobility is defined only in terms of the effective friction where the mobility is independent of the volume.

## 3. Mass-dependent hypermobility of large landslides and debris flows

Observations of large events clearly indicate that when the debris volume exceeds some threshold volume, somewhere in between $V_o = 10^5 \mathrm{m}^3$ to $V_o = 10^7 \mathrm{m}^3$ (Davies and McSaveney, 1999), the total run-out distance is volume-dependent (Howard, 1973; Lucchitta, 1978, 1979; Voight, 1978; Crandell et al., 1984; Francis et al., 1985; Siebert et al., 1987; McEwen, 1989; Stoopes and Sheridan, 1992; Dade and Huppert, 1998; Collins and Melosh, 2003). Observations also reveal contrasting mobilities of different types of events, and even different events of the same type (e.g., volcanic) as indicated by $L/H$. Fig. 2 shows large scatter in the data between volume (eight orders of magnitude) and mobility (three orders of magnitude). Although a positive correlation is observed between avalanche volume ($V_o$) and the measured mobility ($L/H$), it is not clear that event volume systematically controls flow mobility (also see, Davies and McSaveney (1999)). Separating data by event types, Fig. 2 shows that maximum volumes are largest for extraterrestrial events, followed respectively by the submarine, volcanic and non-volcanic events. Volumes range between $10^{-5}$ km$^3$ and $10^5$ km$^3$. Since no systematic relationship exists between the measured $V_o$ and $L/H$, there can be no representative mobility value assigned to a given event volume. Therefore, no clear rule exists for estimating or predicting mobility, requiring quantitative modeling to make meaningful predictions. Quantitative modeling, however, requires a rheological model. In our approach, we developed a rheological model that expresses mobility in terms of the effective Coulomb friction coefficient, resulting in an explicit square-root dependence of inundation area and a cube root dependence of the total volume, Eqs. (6)–(14). As $A$ and $V$ increase, so does the mobility.

As with any analytical model, we compare the model ($1/\mu_e$) given by Eq. (14) to available data ($L/H$) given by Eq. (13) with the best fit values of the parameters. We separate the dataset (see the figure caption for the data references) in Fig. 2 into four categories; extraterrestrial, non-volcanic, volcanic and submarine events in Fig. 3. We define the unified parameter, $U_P = \mu_c (1 - \Lambda) \gamma \mathcal{T} / S^{n-1}$. Here, $U_P$ is associated with $1/\mu_e$ but independent of $L/H$. As in its numerator $N_f$ also contains the gravity constant $g$ via $\tau$, which is in the denominator of $N_f$ (see, Eqs. (6) and (7)). The volume–area slope $S$ in Eq. (8) is thus a non-dimensional quantity. Therefore, $U_P$ can be applied to all event-types. This parameter includes the measure of fluidization $\Lambda$, while the other parameter $\alpha$, in Eq. (15), determines the interpolation between the observed minimum and maximum mean flow depth of an event-type (Dade and Huppert, 1998); $\mathcal{H}_{min} = 2 \times 10^{-3}$km and $\mathcal{H}_{max} = 10^{-2}$km.

We take the best fit values for $U_P$ as follows: $U_P = 90$ for extraterrestrial events, $U_P$ around 18 for terrestrial non-volcanic and volcanic events, and $U_P = 9$ for submarine events. Comparing the large $U_P$ value for the extraterrestrial events (90), the small value for subaerial (18) and very small value for submarine (9), suggests a strong dynamical effect of the fluid pressure where $\Lambda$ values are large. In reality, different events of the same event-type may be associated with different $\Lambda$ values. There can be a set of ($\mu_c, \gamma, \mathcal{T}, \Lambda$ and $S$) values for each event in an event-type. But, the basic and simple analysis presented here shows that the different sets of ($\mu_c, \gamma, \mathcal{T}, \Lambda$ and $S$) values for an event-type should lead to a 'unique' $U_P$ value. The $\alpha$ values are chosen as: 1,1.5,1, and 1 for extraterrestrial, terrestrial non-volcanic and volcanic, and submarine events, respectively. The model prediction with these values is shown for each event type in Fig. 3. Interestingly, since $U_P$ is dominated by the degree of fluidization, where high $U_P$ means low fluidization, the decreasing values are consistent with the degree of fluidization available in each environment. That is, in extraterrestrial environments, low fluidization and high $U_P$ is expected, where high fluidization in submarine environments leads to low $U_P$ values, as observed in Fig. 3. This analysis shows that $\Lambda$ plays a very important role in describing the hypermobility of large volume

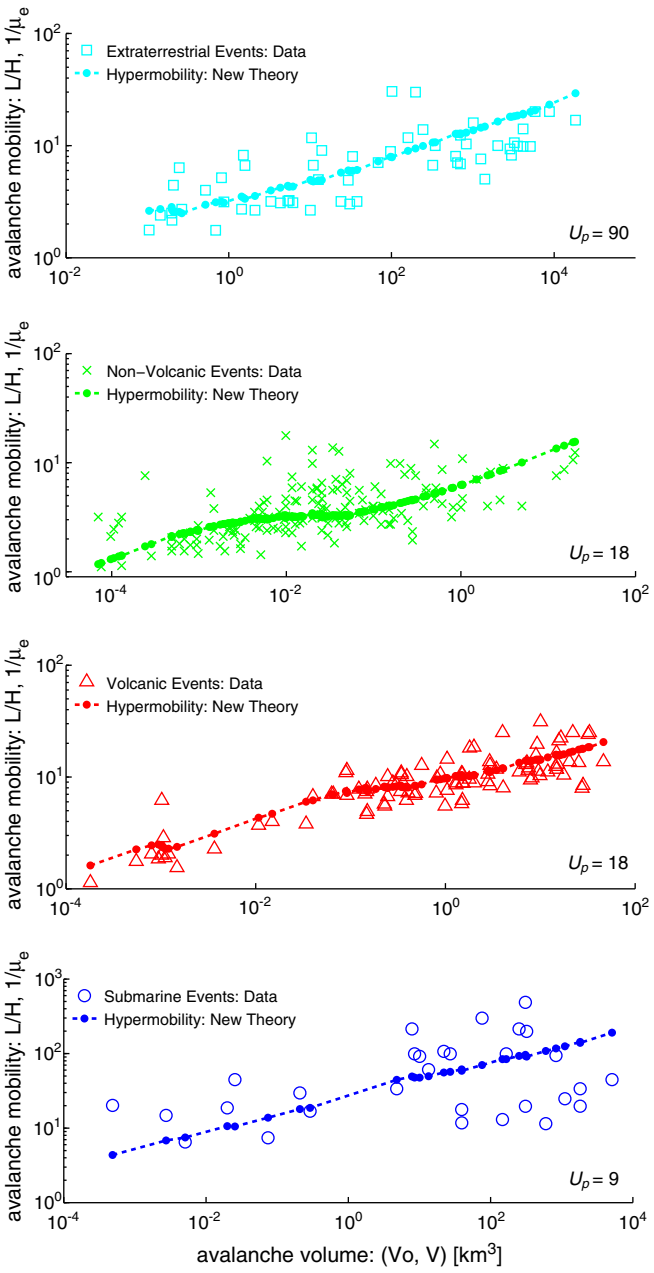


**Fig. 3.** Prediction of hypermobility of extraterrestrial, non-volcanic, volcanic and submarine events in terms of event volumes by the new rheological model for the hypermobility of very large mass flow events. $L/H(=1/\mu_{e_o})$ is the measured hypermobility (in terms of $V_o$) as represented by the symbols (squares, crosses, triangles, and open circles) and $1/\mu_e$ is the model prediction for the hypermobility (as a function of $V$). They are plotted independently as given by Eqs. (13) and (14), respectively. An increasing trend of the hypermobility $1/\mu_e$ with increasing volume ($V$) is observed, and covers the whole range of measured mobility. The filled circles connected by dashed lines are the model predictions. The new hypermobility function well-explains the measured hypermobility. Data as in Fig. 2.

landslides. This also shows that, the fluid pressure for the extraterrestrial flows is about 10% of the normal stress, more than 80% of the normal stress for the non-volcanic and volcanic environments, and more than 90% of the normal stress for the submarine landslides. This means that fluidization is limited in extraterrestrial events, significant fluidization occurs in non-volcanic and volcanic events, and fluidization dominates submarine events. That is, the effects of fluid pressure on landslides mobility are different depending on the environment. This is a new understanding and an important result in terms of describing the hypermobilities of large mass flow events. This may also indicate a very restrictive or even negligible presence and/or effect of water (or possibly fragmentation pressure (Davies et al., 2010)) in the extraterrestrial environment. As mentioned before, significant reductions in the basal shear stress from elevated pore pressures in debris flows is a known phenomenon (Iverson, 1997, 2005; Berti et al., 1999; Major and Iverson, 1999; Iverson and Vallance, 2001; Berti and Simoni, 2005; McArdell et al., 2007). Here, we advance this concept by including the reduced shear stress due to the (excess) pore fluid pressure in describing the hypermobility of huge debris avalanche events. The information of the fluid pressure (through $\Lambda$) is used for the first time to explicitly and analytically explain the unusually long run-out distances of huge avalanches and landslides, and for the different event-types.

Note that $(1/\mu_{e_o} =)L/H$ is the measured hypermobility (data) in terms of the observed volume $V_o$ (Figure 2) and $1/\mu_e$ is the (theoretical–empirical) model prediction for the hypermobility as a function of V. As discussed in Section 2, $L/H$ and $1/\mu_e$ are equivalent but separated and independent of each other. In Fig. 3, both the measured and predicted mobilities are plotted together for a direct comparison. We observe a very good correspondence between the model prediction of $1/\mu_e$ and the data ($L/H$) for all four types of events. Furthermore, the slopes of the prediction curves in Fig. 3 are determined by the model Eqs. (14) and (15).

## 4. Discussion

Typically, small values of the effective friction coefficient ($\mu_e$) are assumed in modeling to explain long runout avalanches and landslides (Legros, 2002). Since our models (6)–(14) depend on mass or volume, they provide a means to implement reduced effective Coulomb friction in the dynamic simulation of very large mass flow events. These models can be used to simulate general mass flow events, develop hazard maps and assess risk, for example, near active volcanoes.

The theoretical–empirical hypermobility function ($1/\mu_e$) systematically explains the mobility of both small and large mass flows, where the volume covers eight orders of magnitude ($10^5$ to $10^{13}$ m$^3$, or even smaller) and the mobility covers about four orders of magnitude ($10^{-1}$ to $10^3$) (Howard, 1973; Lucchitta, 1978, 1979; Voight, 1978; Crandell et al., 1984; Francis et al., 1985; Siebert et al., 1987; McEwen, 1989; Stoopes and Sheridan, 1992; Dade and Huppert, 1998; Legros, 2002; Pudasaini and Hutter, 2007). While it is well-documented that in general the Coulomb concept works well in describing small-sized events in geologic environments and at laboratory scales (see, e.g., Iverson, 1997; Denlinger and Iverson, 2001; Pitman et al., 2003; Pudasaini and Hutter, 2003; Pudasaini and Kroener, 2008; Pudasaini et al., 2005, 2008; Pudasaini and Domnik, 2009; McDougall and Hungr, 2004; Ancey, 2005; Pitman and Le, 2005; Jop et al., 2006; Mangeney et al., 2007) our results demonstrate that the Coulomb friction rheology is also applicable to avalanche events of any size. The method is new, physically-based and successfully validated with a large dataset of huge terrestrial and extraterrestrial avalanche events (Howard, 1973; Lucchitta, 1978, 1979; Voight, 1978; Crandell et al., 1984; Francis et al., 1985; Siebert et al., 1987; McEwen, 1989; Stoopes and Sheridan, 1992; Dade and Huppert, 1998; Capra et al., 2002; Deganutti, 2008).

We further explore the influence of the physical, topographical and volumetric parameters on the mean basal shear stress. In Eq. (6), the shear stress is directly proportional to, and explicitly includes, the Coulomb friction parameter to control the flow dynamics. The mean flow depth, the volume, and the debris overrun area are included to estimate the mean basal shear stress. The shear stress is directly and linearly proportional to the mean flow depth and the flow volume and inversely proportional to the overrun area with power $n>1$. $V$ (or $A$) is the main flow characteristic that largely dominates the flow dynamics. As the data indicate, $A$ increases faster than $V$. $V/A^n<1$ and decreases faster as $V$ increases. This reduces the basal shear stress

and thus enhances the flow mobility. So, as the basal shear stress ($\tau$) controls the flow, $V/A^n$ plays a dominant role for flow mobility. This is in line with the Coulomb friction rheology because the overburden pressure is related to the volume per unit basal area (i.e., depth), which in turn increases the basal shear stress. On the other hand, high flow mobility is associated with increased overrun area. The model (6) can be applied to any shape of the overrun area, and that the estimation of $\tau$ is performed for curved topography in which $\mathcal{T}$ is related to the slope and its curvature. Therefore, no restriction is imposed on the avalanche spreading, which was previously not the case (Dade and Huppert, 1998). Previous models (Dade and Huppert, 1998; Calder et al., 1999; Legros, 2002) were unable to analytically predict the runout extent or distance of the event. Our results quantitatively model and predict the long runout of large debris avalanche events. The explicit form of the mean shear stress model (6) or equivalently the hypermobility function (11) or (14) are important because they can be used to close the Coulomb-type frictional stresses in a continuum description of the entire flow event; from the initiation to the final deposition (Denlinger and Iverson, 2001; Pitman et al., 2003; Pudasaini and Hutter, 2003; Pudasaini and Kroener, 2008; Pudasaini et al., 2005, 2008; Pudasaini and Domnik, 2009; Ancey, 2005; Pitman and Le, 2005; Jop et al., 2006; Mangeney et al., 2007; Pudasaini and Hutter, 2007; Sosio et al., 2011, 2012; Domnik and Pudasaini, 2012). Some models (Dade and Huppert, 1998; Calder et al., 1999; Legros, 2002) argue against the applicability of the Coulomb friction. However, Fig. 3 clearly demonstrates that Coulomb-type friction, often used in the mass flow modeling and simulation for small volumes, is also applicable to large events. For modeling and simulation, the new shear stress model is meaningful because it contains the appropriate physical, topographical and volumetric parameters. We use the real inundation area $A$ or the flow volume $V$ in the derivation of the basal shear stress, the effective mobility function, and other related slopes when compared to the horizontally projected assumed uniform angular area in other models.

The mean shear stress and the effective hypermobility ($1/\mu_e$) are mass-dependent in three different ways; ($a$) on the mean flow height; ($b$) the total flow volume, and ($c$) the total inundation area of the flow. This leads to a strong decrease in the mean shear stress when compared to its local dynamic shear stress, which enhances the flow after the inception and rapidly attains very high momentum. The basal shear stress is so low at the far downstream position that it cannot substantially resist the flow, resulting in the exceptionally long run-out distance. Another possible scenario of the mean basal shear stress is that the entire body may be resisted uniformly over the area in contact with the basal surface, irrespective of the topographic position (Kelfoun and Druitt, 2005; Sosio et al., 2011). Thus, the motion could mainly be sliding or translational as observed in many geological flows of large events (Heim, 1932; Shreve, 1966; Hsu, 1975; Dade and Huppert, 1998; Deganutti, 2008). On the contrary, assuming the gradient of the free surface of the flow, using the local dynamical basal shear stress introduces higher shear resistance below the maximum debris depth. The shear stress would continuously decrease towards the flow margins and to the thinner parts of the moving mass, forcing the center of mass to move relatively slowly (Pudasaini and Hutter, 2007). This induces large shear strains and internal velocity gradients, with the resulting deformation consuming large amounts of energy. This is precisely the point of how the mean frictional shear stress rheology economizes the flow in comparison to the local dynamical basal shear resistance. The essential point is that the theoretical hypermobility function $1/\mu_e$ captures the behavior all event types possess because it empirically includes the volumetric, geometrical and physical parameters that control the event.

Figs. 2 and 3 show that significantly higher mobility values are observed in submarine landslide events, as high as 500, and that the mobility of the extraterrestrial events is relatively low in comparison to the mobility of terrestrial events for the same volume. This indicates that hypermobility is dominated by the degree of fluidization; an intuitive result that is now quantified in our model. Our model quantitatively explains mobility tendencies for each event type. This is important for the prediction of the hypermobility as a function of the volume (or the inundation area) if the release volume can be estimated in advance (see later). Note that area is estimated fairly accurately even for submarine and extraterrestrial events. However, the volumes estimated from the distal thickness are likely to be underestimated. Nevertheless, as the values of the long runout debris avalanches ranges from $10^5$ to $10^{13}$ m$^3$, the uncertainty below order one is generally acceptable for the purpose of analyzing the effect of volume on mobility (Legros, 2002).

Legros (2002) presented systematic data of more than 200 landslides, debris avalanches and debris flows including submarine non-volcanic landslides, submarine volcanic landslides, subaerial volcanic landslides, submarine landslides, and Martian landslides. However, due to the complexity of the events, not all relevant data could be measured. Our models (11) and (14) can estimate (predict) the missing overrun area and volume (see, e.g., Legros, 2002) in terms of the known mobility data ($L/H$), because $\mu_c(1-\Lambda)\gamma\mathcal{T}\mathcal{H}/S^{n-1}$ is constrained by the model validation (see, Figure 3). In most of the cases, mobility is known but volumes and the overrun areas are unknown as they are much more difficult to measure than $L/H$. These models can estimate the missing values, which was not possible with existing mass flow models. Therefore, our model can more accurately predict the event's potential, anticipated hazards, and mapping and mitigation.

Hazards assessments of areas threatened by or under threat of large mass flows (e.g., volcanic collapses, Sosio et al., 2011) need to take into account the extraordinary mobility of the flow. In the modeling and dynamic simulation of avalanches, by applying the geotechnical and geophysical methods, we can first estimate the (potential) avalanche volume (Sosio et al., 2012) or the inundation area and the topographic and the frictional parameters and then determine the effective Coulomb friction $\mu_e$ and the associated hypermobility $1/\mu_e$. Finally, $\mu_e$ can be used to determine the local basal shear stress $\tau_l$, see Eq. (1). The simulation performed with such $\tau_l$ should adequately reproduce the exceptionally long run-out distances associated with very large events.

Comparison of the model against large data sets provides a physical basis for the prediction of the hypermobility of large mass flow events. The new rheological model can be used in the dynamical simulations for the estimation of the flow characteristics and properties, such as the debris inundation areas, depth profile and associated destructive impact forces. The model calibration presented in Section 3 and Fig. 3 shows that the unified parameter $U_P$ lies roughly between 10 and 90, so does the relative fluid pressure (90% to 10%) as compared to the total solid normal stress. As $U_P$ is constrained, we have now some estimates of the $U_P$ values for different event types. Even if we do not have the data for mechanical, dynamical and the geometrical parameters, $\mu_c, \gamma, \mathcal{T}, \Lambda$ and $S$, with these $U_P$ values, we can now estimate the effective friction parameter $\mu_e$ in terms of the volume and the mean flow height. This way, the new model can be used for the prediction of the dynamics of possible avalanches for which there are no data.

## 5. Conclusions

The models presented here for the frictional basal shear stress, effective Coulomb friction coefficient and a hypermobility function successfully describe long runout distances of very large ($>10^6$ m$^3$, by volume) debris avalanche events. These models include the most dominant parameters affecting mobility; the flow volume, the inundation area, the fluidization parameter, and the topographic and frictional parameters in the description of the long run-out lengths. These physically based models systematically describe exceptional mobility

and long run-out distances of huge volume landslides, avalanches, debris flows and rockfalls, and the hypermobility function very well represents the large data set of terrestrial and extraterrestrial events. This model can be used to estimate the overrun area and volume in terms of the known mobility data. We described new independent scaling arguments between the inundation area and the volume based on the arbitrary shape of the inundation area and the mean basal shear stress. Using physical, mathematical, and rheological arguments, this theoretical-empirical model resolves a long-standing issue of describing hypermobility of very large and rapid geophysical events in terms of the volume involved or the inundation area.

*Notation*

| | |
|---|---|
| $A$ | total overrun area/entire landslide area/inundation area. |
| $A_d$ | debris covered area in deposition. |
| $A_t$ | debris covered area at time $t$. |
| $a_c$ | topographically induced centrifugal force. |
| $a_{c_0}$ | maximum of $a_c$. |
| $F$ | effective friction force. |
| $f_A, f_V, f_0$ | functions of area, volume, observed volume. |
| $g$ | gravity acceleration. |
| $H$ | vertical fall height. |
| $\mathcal{H}$ | mean flow depth. |
| $\mathcal{H}_{max}$ | maximum value of $\mathcal{H}$. |
| $\mathcal{H}_{min}$ | minimum value of $\mathcal{H}$. |
| $h$ | flow depth in the direction normal to sliding surface. |
| $L$ | total horizontal runout distance. |
| $N_f$ | friction number. |
| $n$ | a real number $>1$. |
| $S$ | volume-area slope. |
| $\mathcal{T}$ | $= cos\zeta_0 + a_{c_0}$, topographic parameter. |
| $t$ | time. |
| $U_P$ | $= \mu_c(1-\Lambda)\gamma\mathcal{T}/S^{n-1}$, unified parameter. |
| $V$ | debris volume. |
| $V_0$ | observed/measured debris volume. |
| $V_{min}$ | observed minimum value of $V$. |
| $V_{max}$ | observed maximum value of $V$. |
| $W$ | work. |
| $x, y$ | downslope, cross-slope coordinates. |
| $\alpha$ | a parameter. |
| $\gamma$ | $=\gamma_2/\gamma_1$, volumetric parameter. |
| $\gamma_1, \gamma_2$ | proportionality constants. |
| $\Lambda$ | ratio between basal pore fluid pressure and total normal stress. |
| $\mu_c$ | Coulomb friction coefficient. |
| $\mu_e$ | theoretical effective/apparent friction coefficient. |
| $1/\mu_e$ | theoretical hypermobility/hypermobility function. |
| $\mu_{e_o}$ | $=H/L$, observed effective/apparent friction coefficient. |
| $1/\mu_{e_o}$ | $=L/H$, observed hypermobility/mobility data. |
| $\rho$ | bulk density. |
| $\tau$ | mean basal shear stress. |
| $\tau_l$ | local dynamical basal shear stress. |
| $\zeta$ | slope angle of the basal surface. |
| $\zeta_0$ | minimum of $\zeta$. |

## Acknowledgments

Financial support of the German Research Foundation (DFG) through the project PU 386/1-1, PU 386/1-2: *Transition of a Granular Flow into the Deposit* is acknowledged. We are grateful to W. Brian Dade for his comments on the manuscript. We sincerely thank three anonymous referees, and the editor, Giovanni B. Crosta, for their constructive reviews and valuable suggestions that substantially helped to increase the clarity and quality of the paper.

## Appendix A. Mean shear stress

The mean flow depth $\mathcal{H}$ can be estimated as:

$$\mathcal{H} \approx \frac{V}{A_t}. \tag{16}$$

Assuming a power law proportionality between $V$ and $A$, and approximating $A_t$ by $A_d$, Eq. (16) can be written as

$$\mathcal{H} \approx \frac{V}{A_t} \sim \frac{A^n}{A_d}. \tag{17}$$

Again assuming a linear relationship between $A$ and $A_d$, introduce the proportionality relationships as $V=\gamma_1 A^n$ and $A_d=\gamma_2 A$. Then, by defining $\gamma_3=\gamma_1/\gamma_2$, and collecting the exponents with base $A$, Eq. (17) reduces to

$$\mathcal{H} \approx \frac{\gamma_1 A^n}{\gamma_2 A} = \frac{\gamma_1}{\gamma_2} A^{n-1} = \gamma_3 A^{n-1}, \tag{18}$$

where $n>1$ is a real number, $\gamma_1<\gamma_2<1$ are proportionality constants with proper dimensions and $\gamma_3<1$. Therefore, the mean flow depth $\mathcal{H}$ takes the form

$$\mathcal{H} := \gamma_3 A^{n-1}. \tag{19}$$

Eq. (19) means that $\mathcal{H}$ scales with $A^{n-1}$.

With Eqs. (19) and (4) the mean shear stress $\tau$ is obtained in terms of $\mathcal{H}, V$ and $A$ as follows. This is derived in three steps by successive substitutions and simplifications of expressions on the right hand side of Eq. (4). From Eq. (4), we have

$$\tau = \mu_c(1-\Lambda)\rho g \mathcal{T} \frac{V}{A_d}. \tag{20}$$

Multiplying the numerator and denominator by $\mathcal{H}$, we obtain

$$\tau = \mu_c\ (1-\Lambda)\rho g \mathcal{T} \mathcal{H} \frac{V}{A_d}\frac{1}{\mathcal{H}}. \tag{21}$$

From Eqs. (18) and (19) substitute $A_d=\gamma_2 A$ and $\mathcal{H}=\gamma_3 A^{n-1}$, respectively, in the denominator to get

$$\tau = \mu_c(1-\Lambda)\rho g \mathcal{T} \mathcal{H} \frac{V}{\gamma_2 A}\frac{1}{\gamma_3 A^{n-1}}. \tag{22}$$

Since $\gamma_2\gamma_3=\gamma_1$, collecting the exponents with base $A$, we obtain the mean shear stress in terms of $\mathcal{H}, V$ and $A$

$$\tau = \mu_c(1-\Lambda)\frac{\mathcal{T}}{\gamma_1}\rho g \mathcal{H}\frac{V}{A^n}. \tag{23}$$

## Appendix B. Friction number and volume area relationship

Next, we obtain the non-dimensional friction number $N_f$ which is defined as the ratio between the effective normal stress and the shear stress:

$$N_f = \frac{(1-\Lambda)\rho g \mathcal{T} \mathcal{H}}{\tau}. \tag{24}$$

Rearranging the terms representing the effective normal stress and the shear stress, and the terms associated with the area and the

volume, making use of Eq. (23), Eq. (24) can be written as

$$N_f = \frac{\gamma_1}{\mu_c}\frac{A^n}{V}. \tag{25}$$

With the definition of the volume–area slope $S=(N_f\mu_c/\gamma_1)^{1/n}$, Eq. (25) leads to a functional relationship between the volume ($V$) and the area ($A$)

$$A = SV^{1/n}. \tag{26}$$

## Appendix C. Effective Coulomb friction coefficient and hypermobility

In the following, we derive effective Coulomb friction coefficient and hypermobility functions. With simple calculations, this will be achieved at several steps.

Balancing between the work ($W=FL$) and the total available energy ($gMH$), and considering a Coulomb-type friction rheology and applying the shear stress $\tau$ to the debris covered area $A_t$ (equivalently, $A_d$) to obtain the friction force, $F=\tau A_d$, we have

$$gMH = FL = \tau A_d L. \tag{27}$$

Substituting for $\tau$ from Eq. (23), we obtain

$$gMH = \mu_c(1-\Lambda)\frac{\mathcal{T}}{\gamma_1}\rho g\mathcal{H}\frac{V}{A^n}A_d L. \tag{28}$$

In the following, to obtain the effective Coulomb friction coefficient, we mainly substitute, rearrange relevant terms and simplify some expressions on the right hand sides at several steps. Since $A_d=\gamma_2 A$, it follows

$$gMH = \mu_c(1-\Lambda)\frac{\mathcal{T}}{\gamma_1}\rho g\mathcal{H}\frac{V}{A^n}\gamma_2 A L. \tag{29}$$

Collecting the volumetric expression ($g\rho VL$), and the parameters $\gamma_1$ and $\gamma_2$, and collecting the exponents in $A$, leads to

$$gMH = (g\rho VL)\mu_c(1-\Lambda)\frac{\gamma_2}{\gamma_1}\mathcal{T}\frac{\mathcal{H}}{A^{n-1}}. \tag{30}$$

Defining $\gamma=\gamma_2/\gamma_1=1/\gamma_3$, and since $M=\rho V$, where $M$ is the debris mass, $\rho$ is the bulk density, and $V$ is the debris volume, we have

$$gMH = (gML)\mu_c(1-\Lambda)\gamma\mathcal{T}\frac{\mathcal{H}}{A^{n-1}}. \tag{31}$$

Now, dividing both sides by $gML$, we obtain an equivalent relationship between $\frac{H}{L}$ and $\mu_c(1-\Lambda)\gamma\mathcal{T}\frac{\mathcal{H}}{A^{n-1}}$. By denoting $\mu_c(1-\Lambda)\gamma\mathcal{T}\frac{\mathcal{H}}{A^{n-1}}$ by $\mu_e$, Eq. (31) leads to ($\equiv$ stands for equivalent)

$$\frac{H}{L} \equiv \mu_c(1-\Lambda)\gamma\mathcal{T}\frac{\mathcal{H}}{A^{n-1}} =: \mu_e. \tag{32}$$

We know that $H/L$ is the observed quantity (effective or apparent friction coefficient) that is somehow related to the observed volume ($V_o$) (see Figure 2). Here, 'o' stands for observed quantity with discrete distribution. So, there should exist a (unknown) functional relation ($f_o$) between $V_o$ and $H/L$, i.e., $H/L=f_o(V_o)$. With this, Eq. (32) can be written as

$$f_o(V_o) = \frac{H}{L} \equiv \mu_c(1-\Lambda)\gamma\mathcal{T}\frac{\mathcal{H}}{A^{n-1}} = \mu_e. \tag{33}$$

Let $\mu_{e_o}$ be the effective friction coefficient as a function of the observed volume ($V_o$). Since $\mu_c(1-\Lambda)\gamma\mathcal{T}\frac{\mathcal{H}}{A^{n-1}}$ is an expression in $A$, a functional relation $f_A$ can formally be assigned to this expression. With these notations, the equivalent expressions in Eq. (33) can be separated as

$$\mu_{e_o} := f_o(V_o) = \frac{H}{L}, \tag{34}$$

$$\mu_e = \mu_c(1-\Lambda)\gamma\,\mathcal{T}\frac{\mathcal{H}}{A^{n-1}} =: f_A(A). \tag{35}$$

Note that in the above expressions, $\mu_{e_o}$ and $f_A$ are introduced only for notational convenience.

Next important step is to obtain a relationship similar to Eq. (35) in terms of the debris volume, $V$. Combining Eqs. (26) and (32) produces a functional relationship between the debris volume and the theoretical hypermobility (defined as $1/\mu_e$) which can be re-written in terms of $V$ as:

$$\frac{H}{L} \equiv \frac{\mu_c(1-\Lambda)\gamma\,\mathcal{T}}{S^{n-1}}\frac{\mathcal{H}}{V^{1-\frac{1}{n}}} := \mu_e. \tag{36}$$

Since $\frac{\mu_c(1-\Lambda)\gamma\,\mathcal{T}}{S^{n-1}}\frac{\mathcal{H}}{V^{1-\frac{1}{n}}}$ is an expression in $V$, as discussed above, a functional relation $f_V$ can formally be assigned to this expression. As in Eqs. (34) and (35), equivalent expressions in Eq. (36) can be separated as

$$\mu_{e_o} = f_o(V_o) = \frac{H}{L}, \tag{37}$$

$$\mu_e = \frac{\mu_c(1-\Lambda)\gamma\mathcal{T}}{S^{n-1}}\frac{\mathcal{H}}{V^{1-\frac{1}{n}}} := f_V(V). \tag{38}$$

Eq. (38) (similarly, Eq. (35)) represents an explicit and theoretical–empirical functional relation for $\mu_e$ (theoretical effective or apparent friction coefficient) in terms of the (continuous) volume (distribution), $V$.

## References


Ancey, C., 2005. Monte Carlo calibration of avalanches as a Coulomb fluid. Philosophical Transactions of the Royal Society A 363, 1529–1550.

Beget, J.E., Kienle, J., 1992. Cyclic formation of debris avalanches at Mount St Augustine volcano. Nature 356, 701–704.

Berti, M., Simoni, A., 2005. Experimental evidences and numerical modeling of debris flow initiated by channel runoff. Landslides 2, 171–182.

Berti, M., Genevois, R., Simoni, A., Tecca, P.R., 1999. Field observations of a debris flow event in the Dolomites. Geomorphology 29, 265–274.

Cagnoli, B., Quareni, F., 2009. Oscillation-induced mobility of flows of rock fragments with quasi-rigid plugs in rectangular channels with frictional walls: a hypothesis. Engineering Geology 103 (1–2), 23–32.

Calder, E.S., Cole, P.D., Dade, W.B., Druitt, T.H., Hoblitt, R.P., Huppert, H.E., Ritchie, L., Sparks, R.S.J., Young, S.R., 1999. Mobility of Pyroclastic flows and surges at the Soufriere Hills Volcano, Montserrat. Geophysical Research Letters 26, 537–540.

Campbell, C.S., 2006. Granular material flows — an overview. Powder Technology 162, 208–229.

Capra, L., Macias, J.L., Scott, K.M., Abrams, M., Garduno-Monroy, V.H., 2002. Debris avalanches and debris flows transformed from collapses in the Trans-Mexican Volcanic Belt, Mexico-behavior, and implications for hazard assessment. Journal of Volcanology and Geothermal Research 113, 81–110.

Collins, G.S., Melosh, H.J., 2003. Acoustic fluidization and the extraordinary mobility of sturzstroms. Journal of Geophysical Research 108 (B10), 2473. http://dx.doi.org/10.1029/2003JB002465.

Crandell, D.R., Miller, C.D., Glicken, H.X., Christiansen, R.L., Newhall, C.G., 1984. Catastrophic debris avalanche from ancestral Mount Shasta volcano. California Geology 12, 143–146.

Dade, W.B., Huppert, H.E., 1998. Long-runout rockfall. Geology 26, 803–806.

Davies, T.R.H., 1982. Spreading of rock avalanche debris by mechanical fluidization. Rock Mechanics 15, 9–24.

Davies, T.R., McSaveney, M.J., 1999. Runout of dry granular avalanches. Canadian Geotechnical Journal 36 (2), 313–320.

Davies, T., McSaveney, M., Kelfoun, K., 2010. Runout of the Socompa volcanic debris avalanche, Chile: a mechanical explanation for low basal shear resistance. Bulletin of Volcanology 72 (8), 933–944.

Deganutti, A.M., 2008. The hypermobility of rock avalanches. (PhD Dissertation, Universita delgi Studi di Padova).

Denlinger, R.P., Iverson, R.M., 2001. Flow of variably fluidized granular masses across three-dimensional terrain: 2. Numerical predictions and experimental tests. Journal of Geophysical Research 106 (B1), 553–566.
Domnik, B., Pudasaini, S.P., 2012. Full two-dimensional rapid chute flows of simple viscoplastic granular materials with a pressure-dependent dynamic slip-velocity and their numerical simulations. Journal of Non-Newtonian Fluid Mechanics 173–174, 72–86.
Fischer, J.T., Kowalski, J., Pudasaini, S.P., 2012. Topographic curvature effects in applied avalanche modeling. Cold Regions Science and Technology 74–75, 21–30.
Francis, P.W., Gardeweg, M., O'Callaghan, L.J., Ramirez, C.F., Rothery, D.A., 1985. Catastrophic debris avalanche deposit of Socampa volcano, north Chile. Geology 13, 600–603.
Heim, A., 1932. Der Bergsturz und Menschenleben. Fretz und Wasmuth Verlag, Zürich.
Howard, K.A., 1973. Avalanche mode of motion: implications from lunar examples. Science 180, 1052–1055.
Hsu, K.J., 1975. Catastrophic debris stream (Sturzstroms) generated by rockfalls. Geological Society of America Bulletin 86, 129140.
Hungr, O., 1990. Mobility of rock avalanches: Report of National Research Institute for Earth Science and Disaster Prevention, Japan, 46, pp. 11–19.
Iverson, R.M., 1997. The physics of debris flows. Reviews of Geophysics 35 (3), 245–296.
Iverson, R.M., 2005. Regulation of landslide motion by dilatancy and pore pressure feedback. Journal of Geophysical Research 110, F02015. http://dx.doi.org/10.1029/2004JF000268.
Iverson, R.M., Denlinger, R.P., 2001. Flow of variably fluidized granular masses across three-dimensional terrain: 1. Coulomb mixture theory. Journal of Geophysical Research 106 (B1), 537–552.
Iverson, R.M., Vallance, J.W., 2001. New views of granular mass flows. Geology 29, 115–118.
Jop, P., Forterre, Y., Pouliquen, O., 2006. A constitutive law for dense granular flow. Nature 441, 727–730.
Keefer, D.K., 1984. Rock avalanches caused by earthquakes: source characteristics. Science 223, 1288–1289.
Kelfoun, K., Druitt, T.H., 2005. Numerical modeling of the emplacement of Socompa rock avalanche, Chile. Journal of Geophysical Research 110, B12202. http://dx.doi.org/10.1029/2005JB003758.
Kent, P.E., 1966. The transport mechanism in catastrophic rock falls. Journal of Geology 74, 79–83.
Legros, F., 2002. The mobility of long runout landslides. Engineering Geology 63, 301–331.
Lucas, A., Mangeney, A., 2007. Mobility and topographic effects for large Valles Marineris landslides on Mars. Geophysical Research Letters 34, L10201. http://dx.doi.org/10.1029/2007GL029835.
Lucchitta, B.K., 1978. A large landslide on Mars. Geological Society of America Bulletin 89, 1601–1609.
Lucchitta, B.K., 1979. Landslides in Valles Marineris, Mars. Journal of Geophysical Research 84, 8097–8113.
Major, J., Iverson, R.M., 1999. Debris-flow deposition: effects of pore-fluid pressure and friction concentrated at flow margins. Geological Society of America Bulletin 110, 1424–1434.
Mangeney, A., Tsimring, L.S., Volfson, D., Aranson, I.S., Bouchut, F., 2007. Avalanche mobility induced by the presence of an erodible bed and associated entrainment. Geophysical Research Letters 34, L22401.
McArdell, B.W., Bartelt, P., Kowalski, J., 2007. Field observations of basal forces and fluid pore pressure in a debris flow. Geophysical Research Letters 34, L07406. http://dx.doi.org/10.1029/2006GL029183.
McDougall, S., Hungr, O., 2004. A model for the analysis of rapid landslide motion across three-dimensional terrain. Canadian Geotechnical Journal 41 (6), 1084–1097.
McEwen, A.S., 1989. Mobility of large rock avalanches: evidence from Valles Marineris, Mars. Geology 17, 1111–1114.
McSaveney, M.J., 1978. Sherman glacier rock avalanche, Alaska, U.S.A. In: Voight, B. (Ed.), Natural Phenomena. Rockslides and Avalanches, vol. 1. Elsevier Sci., New York, pp. 197–258.
McSaveney, M.J., Davies, T.R.H., 2009. Surface energy is not one of the energy losses in rock comminution. Engineering Geology 109, 109–113.
Middleton, G.V., Wilcock, P.R., 1994. Mechanics in the Earth and Environmental Sciences. Cambridge University Press, Cambridge, UK.
Okura, Y., Kitahara, H., Kawanami, A., Kurokawa, U., 2003. Topography and volume effects on travel distance of surface failure. Engineering Geology 67 (3–4), 243–254.
Pitman, E.B., Le, L., 2005. A two-fluid model for avalanche and debris flows. Philosophical Transactions of the Royal Society A 363, 1573–1602.
Pitman, E.B., Nichita, C.C., Patra, A., Bauer, A., Sheridan, M.F., Bursik, M., 2003. Computing debris flows and landslides. Physics of Fluids 15 (12), 3638–3646.
Pudasaini, S.P., 2012. A general two-phase debris flow model. Journal of Geophysical Research 117, F03010. http://dx.doi.org/10.1029/2011JF002186.
Pudasaini, S.P., Domnik, B., 2009. Energy consideration in accelerating rapid shear granular flows. Nonlinear Processes in Geophysics 16, 399–407.
Pudasaini, S.P., Hutter, K., 2003. Rapid shear flows of dry granular masses down curved and twisted channels. Journal of Fluid Mechanics 495, 193–208.
Pudasaini, S.P., Hutter, K., 2007. Avalanche Dynamics: Dynamics of Rapid Flows of Dense Granular Avalanches. Springer Berlin, New York.
Pudasaini, S.P., Kroener, C., 2008. Shock waves in rapid flows of dense granular materials: theoretical predictions and experimental results. Physical Review E 78 (4). http://dx.doi.org/10.1103/PhysRevE.78.041308.
Pudasaini, S.P., Wang, Y., Hutter, K., 2005. Modelling debris flows down general channels. Natural Hazards and Earth System Sciences 5, 799–819.
Pudasaini, S.P., Wang, Y., Sheng, L.-T., Hsiau, S.-S., Hutter, K., Katzenbach, R., 2008. Avalanching granular flows down curved and twisted channels: theoretical and experimental results. Physics of Fluids 20 (7), 073302. http://dx.doi.org/10.1063/1.2945304.
Shreve, R.L., 1966. Sherman Landslide, Alaska. Science 154, 1639–1643.
Siebert, L., 1992. Threats from debris avalanches. Nature 356, 658–659.
Siebert, L., Glicken, H., Ui, T., 1987. Volcanic hazards from Bezymianny- and Bandai-type eruptions. Volcanology Bulletin 49, 435–459.
Sosio, R., Crosta, G.B., Hungr, O., 2011. Numerical modeling of debris avalanche propagation from collapse of volcanic edifices. Landslides 9, 315–334.
Sosio, R., Crosta, G.B., Chen, J.H., Hungr, O., 2012. Modelling rock avalanche propagation onto glaciers. Quaternary Science Reviews 47, 23–40.
Stoopes, G.R., Sheridan, M.F., 1992. Giant debris avalanches from the Colima Volcanic Complex, Mexico: implications for long-runout landslides (>100 km) and hazard assessment. Geology 20, 299–302.
Strom, A.L., 2006. Morphology and internal structure of rockslides and rock avalanches; grounds and constraints for their modelling. In: Evans, S.G., Scarascia-Mugnozza, G., Strom, A.L., Hermanns, R.L. (Eds.), Landslides from Massive Rock Slope Failure. NATO Science Series: IV, Earth and Environmental Sciences. Springer, Dordrecht, pp. 305–326.
Vallance, J.W., Scott, K.M., 1997. The Osceola Mudflow from Mount Rainier; sedimentology and hazard implications of a huge clay-rich debris flow. Geological Society of America Bulletin 109, 143–163.
Voight, B., 1978. Rockslides and Avalanches, vol. 1. Elsevier, New York.
Voight, B., 1988. A method for prediction of volcanic eruptions. Nature 332, 125–130.